LAWRENCE
LIVERMORE
NATIONAL
LABORATORY

Role of Hydrodynamics Simulations in Laser-Plasma Interaction Predictive Capability

N. B. Meezan, R. L. Berger, L. Divol, D. H. Froula, D. E. Hinkel, O. S. Jones, R. A. London, J. D. Moody, M. M. Marinak, C. Niemann, P. B. Neumayer, S. T. Prisbrey, J. S. Ross, E. A. Williams, S. H. Glenzer, L. J. Suter

November 8, 2006

Disclaimer

Role of hydrodynamics simulations in laser-plasma interaction predictive capability

N. B. Meezan,* R. L. Berger, L. Divol, D. H. Froula, D. E. Hinkel, O. S. Jones, R. A. London, J. D. Moody, M. M. Marinak, C. Niemann,† P. B. Neumayer, S. T. Prisbrey, J. S. Ross, E. A. Williams, S. H. Glenzer, and L. J. Suter

Lawrence Livermore National Laboratory, P.O. Box 808, Livermore, CA, 94551-0808

Efforts to predict and control laser-plasma interactions (LPI) in ignition hohlraum targets for the National Ignition Facility [G. H. Miller *et al.*, Optical Eng. **43**, 2841 (2004)] are based on plasma conditions provided by radiation hydrodynamic simulations. Recent experiments provide compelling evidence that codes such as HYDRA [M. M. Marinak *et al.*, Phys. Plasmas **8**, 2275 (2001)] can accurately predict the plasma conditions in laser heated targets such as gas-filled balloon (gasbag) and hohlraum platforms for studying LPI. Initially puzzling experimental observations are found to be caused by bulk hydrodynamic phenomena. Features in backscatter spectra and transmitted light spectra are reproduced from the simulated plasma conditions. Simulations also agree well with Thomson scattering measurements of the electron temperature. The calculated plasma conditions are used to explore a linear-gain based phenomenological model of backscatter. For long plasmas at ignition-relevant electron temperatures, the measured backscatter increases monotonically with gain and is consistent with linear growth for low reflectivities. These results suggest a role for linear gain postprocessing as a metric for assessing LPI risk.

I. INTRODUCTION

The National Ignition Facility (NIF) [1] is designed to achieve fusion ignition using the inertial confinement fusion (ICF) scheme [2]. Successful indirect drive ignition on the NIF requires controlling laser-plasma interactions (LPI) such as stimulated backscatter and the filamentation instability. In indirect drive ICF, a pellet containing fusion fuel is placed inside a radiation cavity, or hohlraum, that is heated by multiple laser beams. Backscatter and other LPI can prevent the hohlraum from reaching the x-ray drive necessary to symmetrically implode the pellet. To prevent this, designs for NIF ignition hohlraums undergo LPI risk assessments. A variety of theoretical and computational LPI predictive tools are available for risk assessment [3], and all such tools rely on accurate radiation-hydrodynamics calculations of target plasma conditions. The simulation codes must be validated to provide confidence in their abilities to predict ignition hohlraum plasma conditions.

In this paper, we present detailed comparisons of radiation-hydrodynamics simulations performed with the code HYDRA to experimental measurements of plasma conditions inside laser-heated targets. This study spans a wide variety of targets and diagnostic techniques, including gas-filled balloons (gasbags) illuminated by a single laser, gasbags heated by multiple laser beams, and hohlraums heated by multiple laser beams (Fig. 1). The plasma conditions predicted by HYDRA generally agree with direct Thomson scattering measurements of the electron temperature and with indirect measurements,

such as x-ray emission images, backscattered light spectra, and transmitted light spectra.

By analyzing the HYDRA results with a linear gain postprocessor, we can reproduce features seen in experimental time-resolved backscattered light spectra. The agreement between simulation and experiment suggests that we can use backscattered light spectra to diagnose bulk plasma conditions inside laser-heated targets. Although hydrodynamics simulations and linear gain postprocessing do not constitute a complete LPI predictive capability, we find that the stimulated Brillouin backscatter (SBS) measured in experiments performed at ignition hohlraum relevant electron temperatures is consistent with linear growth for reflectivities below 40 %. These results suggest that linear gain postprocessing can be a useful technique for assessing backscatter risk in ignition hohlraums.

II. SIMULATION CAPABILITIES

The massively parallel, three-dimensional radiation-hydrodynamics code HYDRA handles the essential physics for simulating ICF targets [4]. HYDRA uses an arbitrary Lagrangian-Eulerian hydrodynamics scheme that allows computationally efficient simulation of complex geometries. The laser raytrace package accounts for refraction and collisional absorption and includes ponderomotive effects. Multigroup diffusion and Monte Carlo photonics packages are available for radiation transport, with LTE (local thermodynamic equilibrium) opacity tables or an in-line non-LTE opacity model [5]. The HYDRA simulations described in this paper were run in two-dimensional axisymmetric geometry on a single processor.

─────────

*Electronic address: meezan1@llnl.gov
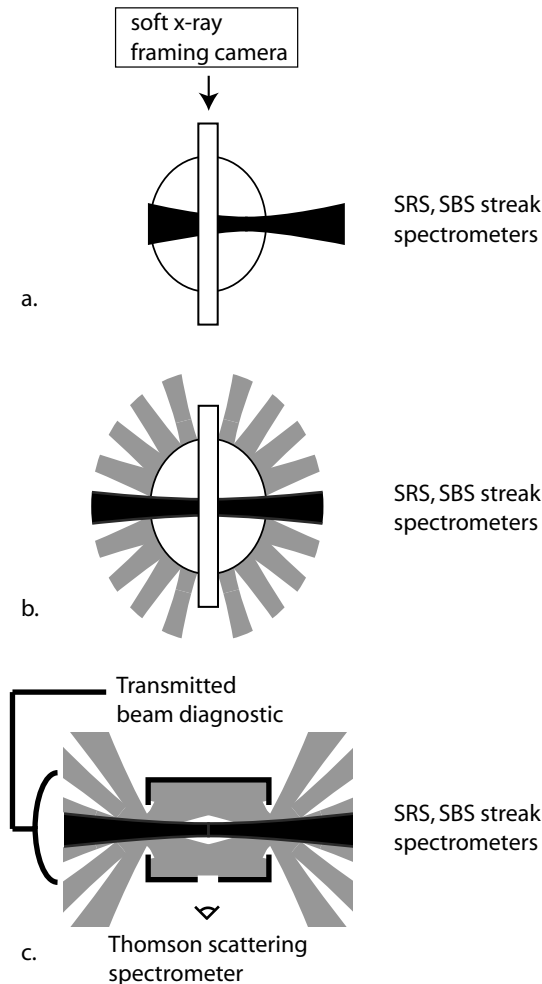†also at the University of California Los Angeles

FIG. 1: Schematics of three types of laser plasma interaction targets. (a) A single 2ω beam propagates through a HELEN gasbag. (b) An OMEGA gasbag is pre-heated by 3ω beams before the 2ω interaction beam turns on. (c) An OMEGA gas-filled hohlraum is pre-heated by 3ω beams and can have a 2ω or 3ω interaction beam.

A. Electron thermal conduction

In HYDRA, electron thermal conduction is handled either with flux-limited diffusion or with the Schurtz, Nicolaï and Busquet (SNB) multi-group nonlocal transport model [6]. The flux-limiter is an adjustable parameter used to limit the classical heat transport to some fraction f of the free-streaming heat flux, as classical heat transport can be unphysical for large temperature gradients. A more detailed discussion of heat transport in hohlraum calculations can be found in Ref. [7]. Historically, calculations of hohlraum targets using $f = 0.05$ have agreed well with experimental measurements of radiation drive and symmetry [8], so this value is used for the vast majority of NIF ignition design calculations. Since we are trying to validate the simulations for NIF ignition calculations, we show results from hohlraum sim-

ulations with $f = 0.05$.

Recent experiments have shown that $f = 0.05$ is inappropriate for "open" geometry targets such as gas jets [9] and gas balloons [10]. Nonlocal transport models give good results for these targets. Simulations of gas balloon experiments with near-classical transport ($f = 1$) gave reasonable results similar to the SNB nonlocal model, whereas $f = 0.05$ was clearly wrong [10]. It appears that $f = 0.05$ approximates the reduction in heat flux that occurs between the hohlraum wall and any gas fill due to non-local transport, or possibly due to self-generated magnetic fields or other effects. In open targets where the heat transport is not dominated by a high density wall with steep density and temperature gradients, classical transport does reasonably well.

B. Linear gain postprocessor

Simulations from HYDRA can be compared to time-resolved backscatter spectra using linear gain postprocessing. The laser interaction postprocessor NEWLIP [11] calculates the steady-state convective spatial growth rate for stimulated Raman backscatter (SRS) and Brillouin backscatter (SBS) as a function of the scattered light frequency ω_s,

$$g\left(\omega_s, x\right) = \frac{1}{2}\left(\frac{v_0}{c}\right)^2 \frac{k_w^2}{k_s} \text{Im}\left[\frac{\chi_e\left(1 + \chi_i\right)}{1 + \chi_e + \chi_i}\right]. \qquad (1)$$

Here, v_0 is the oscillatory velocity of an electron in the laser electric field, c is the speed of light, k_w is the wavenumber of the excited wave (Langmuir wave for SRS, ion acoustic wave for SBS), k_s is the wavenumber of the backscattered light, and χ_e and χ_i are the kinetic expressions for the electron and ion susceptibilities, respectively [12, 13].

Plasma properties are extracted from rays traced through the simulation mesh. At each time, the growth rate $g\left(\omega_s, x\right)$ is integrated along each ray to give the total backscatter gain,

$$G\left(\omega_s\right) = 2\int_{\text{ray}} g\left(\omega_s, x\right) dx. \qquad (2)$$

Here, G refers to the gain for the intensity of the scattered light wave—hence the factor of two. The gain is averaged over multiple rays to reduce noise (ray effects) from the hydrodynamics calculation. Comparisons of the spatial gain g to the simulated plasma properties and composition along the ray can locate regions of high backscatter risk. Thus, an experimental backscatter spectrum can be compared to the "gain spectrum" $G\left(\omega_s, t\right)$ to reveal the spatial origin of the measured backscatter.
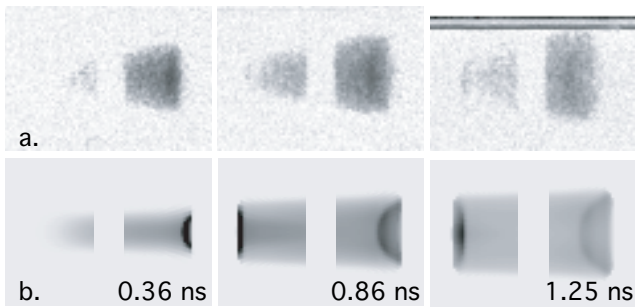
FIG. 2: (a) Side-on gated soft x-ray images show laser propagation across a HELEN gasbag. (b) Simulated images from HYDRA reproduce the shapes of the experimental images.

III. LPI EXPERIMENTS

A. Single-beam gasbag experiments

Experiments were conducted at the HELEN laser facility [14] to study the propagation of a 2ω laser beam. These experiments have been described in greater detail in previous papers [10, 15]. A schematic of the experimental setup at HELEN is shown in Fig. 1(a). A gasbag consists of an aluminum washer with a thin plastic skin bonded to each end. When inflated, a gasbag forms an ellipsoid ≈ 2.4 to 2.5 mm long. The gasbags were filled with hydrocarbon (CH) gas. The laser beam delivered up to 400 J of energy in a 1 ns square pulse to the target. A phase-zone plate [16] was used to generate a 250 μm diameter laser spot. A gated soft x-ray framing camera captured the beam propagating through the target at three times, while SRS and SBS streak spectrometers recorded the backscattered light spectra.

Figure 2 compares x-ray images of a gasbag with initial density $n_e = 0.15\,n_c$ (2ω) to HYDRA simulations run with the SNB nonlocal electron transport model. The simulated images matched the shapes seen in the experimental images and the extent of the beam propagation, within the timing uncertainty of the x-ray framing camera. Simulations with flux-limited diffusion and $f = 1$ were similar [10]. Figure 3(a) shows the measured SRS streak spectrum for the same target. The SRS gain spectrum from NEWLIP [Fig. 3(b)] reproduced the main features of the measured spectrum. The shape of the SRS spectrum correlated directly to the temperature and density profiles in the plasma. Figure 3(c) shows simulated lineouts of the electron density n_e along the beam axis (electron temperature is not shown). The position of each marker in Fig. 3(b) corresponds to the wavelength of peak SRS gain at the simulated (n_e, T_e). This result indicated that the measured spectrum could be used as a diagnostic for the bulk plasma conditions in the laser-beam channel.
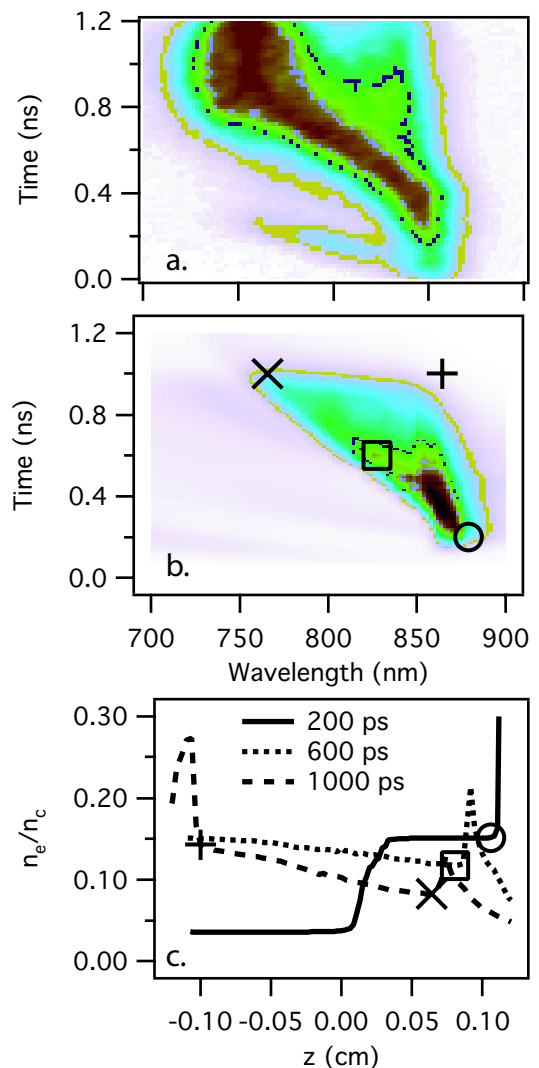

FIG. 3: (Color online). (a) The experimental SRS streak spectrum for a HELEN gasbag of initial density $n_e = 0.15\,n_c$ is tilted towards $\lambda_0 = 527$ nm and broadens in wavelength over time. (b) The simulated SRS (gain) streak spectrum from HYDRA and NEWLIP shows similar behavior. (c) Simulated profiles of n_e along the beam axis at three times correspond directly to features in the simulated spectrum.

B. Multi-beam gasbag experiments

In the single beam experiments, the intensity of the interaction beam could not be varied without changing the plasma conditions. In multi-beam gasbags experiments performed on the OMEGA laser [17], the interaction beam delivered a small fraction (400 J) of the total energy (10–18 kJ), so its intensity (and smoothing) could be varied independently of the background plasma conditions. These experiments are described in more detail in a previous paper [18]. A continuous phase plate (CPP) focused the interaction laser to a 200 μm diameter spot at the center of the gasbag. Calorimeters and streaked spec-
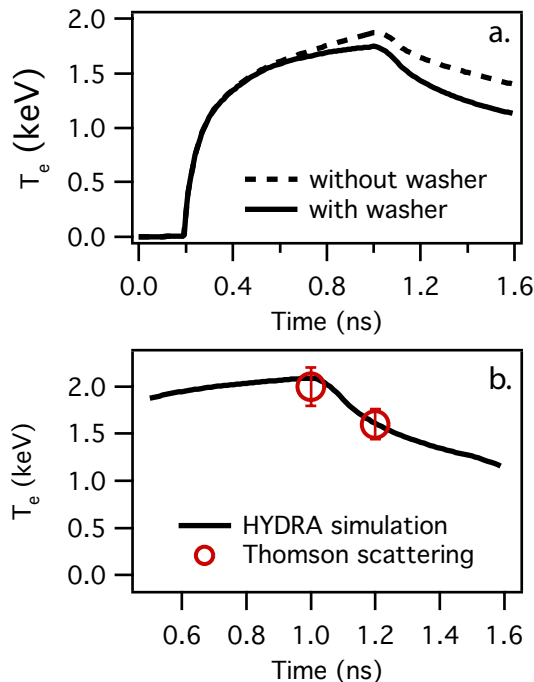
FIG. 4: (Color online). (a) The calculated electron temperature T_e at the center of a multi-beam OMEGA gasbag decreased by ≈ 20 % when the aluminum washer was included in the simulation. (b) HYDRA simulations using a flux limiter of $f = 1$ agreed well with Thomson scattering measurements.
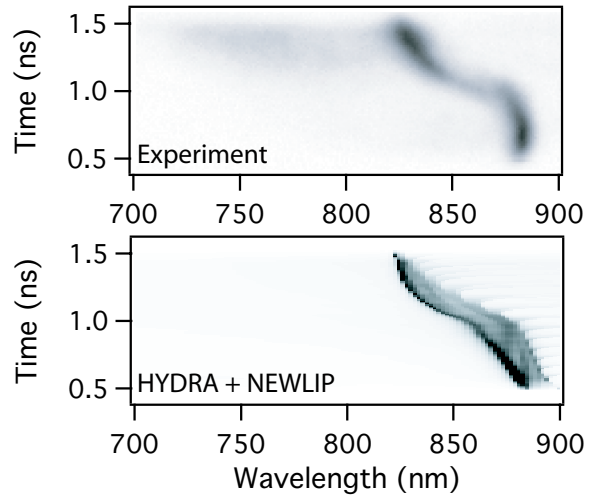

FIG. 5: The experimental SRS streak spectrum from an OMEGA gasbag with a 2ω interaction beam shifted from $\lambda \approx 880$ nm to $\lambda \approx 825$ nm at 1 ns, when the heater beams were turned off. (b) This spectral feature was reproduced in detail by HYDRA and NEWLIP.

trometers measured the SRS and SBS backscatter from the 2ω interaction beam. The gasbags were filled with a hydrocarbon gas mixture to reach an electron density $n_e \approx 14$ % of the critical density (2ω).

It was necessary to include the aluminum washer in the HYDRA simulations of these targets: the washer acted as a heat sink, removing energy from the plasma via thermal conduction (this was not needed for the HELEN experiments, as the laser pulse ended before the heat-wave reached the washer). As shown in Fig. 4(a), including the washer in the simulations lowered the electron temperature at the center of the gasbag by approximately 250 eV (20 %). On some shots, the 2ω beam was used as a Thomson scattering probe to measure the electron temperature [19]. Figure 4(b) shows good agreement between the Thomson scattering data and HYDRA simulations with the aluminum washer included and a flux limiter of $f = 1$ (note that $f = 1$ is practically equivalent to classical Spitzer-Harm transport). Simulations of this target using the SNB non-local model were similar to $f = 1$ simulations—within 10% in electron temperature. In the non-local simulations, ray-effects led to statistical spatial variations in the electron temperature [20], so we show $f = 1$ results here.

In these experiments, the backscatter was dominated by SRS: SBS reflectivity was generally below 1%. The experimental 2ω SRS spectrum, shown in Fig. 5(a), showed

a sudden shift towards $\lambda_0 = 527$ nm around 1 ns, when the 3ω heater beams began to shut off. Postprocessed NEWLIP spectra from HYDRA simulations reproduced this feature [Fig. 5(b)]. In simulations, the gasbag was hottest at the center, so n_e dropped to restore pressure balance. This hydrodynamic expansion combined with the rapid drop in T_e after the heater beams turned off to shift the spectrum to lower wavelength. The agreement between simulation and experiment indicated that the measured SRS backscatter came from the gasbag plateau, the part of the target designed to emulate ignition hohlraum plasma conditions.

On some shots in the campaign, additional smoothing techniques were used on the interaction beam, e.g., polarization smoothing (PS) and smoothing by spectral dispersion (SSD). Beam smoothing improved the propagation of the interaction beam [18] but did not affect the shape of the SRS spectra, supporting the argument that the spectral shape is due to bulk hydrodynamics. While the SRS spectrum showed qualitative agreement with linear theory, a quantitative assessment of reflectivity versus gain was not possible. The hydrodynamics of gasbags is largely dominated by the inward-running blast waves driven by the initial explosion of the bag membrane by the laser [21], and the 2ω laser is strongly absorbed in the high-density peaks. The SRS backscattered light is also strongly absorbed, so small errors in the calculated density of the blast wave peaks result in very large errors in the measured SRS and in the predicted gain.
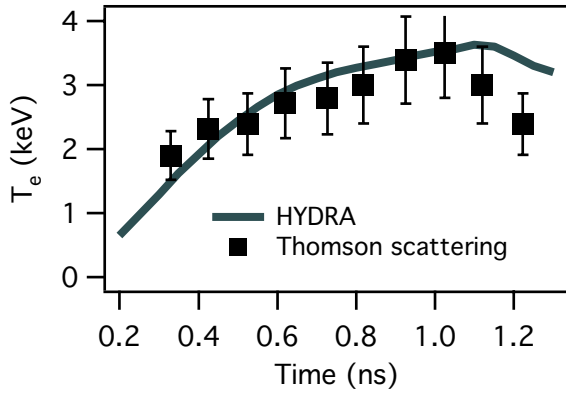
FIG. 6: The simulated electron temperature at the center of an OMEGA gas-filled hohlraum agreed well with Thomson scattering measurements.

C. Gas-filled hohlraum experiments

A new target has been developed for LPI experiments at ignition-relevant electron temperatures on the OMEGA laser [7]. A schematic of this target is shown in Fig. 1(c). This target was configured for experiments with a 2ω or 3ω interaction beam. For experiments with a 2ω interaction beam, the hohlraum was filled with a hydrocarbon gas mixture to reach an electron density $n_e \approx 0.14\ n_c$. A continuous phase plate (CPP) focused the interaction beam to a spot diameter of 200 μm. The shots described here did not use PS or SSD. The interaction beam was generally delayed by $t_0 = 0.3$ ns relative to the heater beams.

For some shots, the 2ω interaction beam was replaced with a 4ω Thomson scattering probe laser. As shown in Fig. 6, HYDRA calculations of the electron temperature in the scattering volume agreed well with the measurements. These simulations used a flux limiter of $f = 0.05$. Calculations using the SNB nonlocal model agreed equally well with the Thomson scattering data. Unfortunately, the Thomson scattering experiment was not sufficient to differentiate beween the two models (see Ref. [7], Fig. 2 and Fig. 5). As mentioned above, most NIF ignition calculations are done with $f = 0.05$, so validating the simulations for this setting is prudent.

In contrast to the gasbags, the backscatter from the hohlraums was dominated by SBS. The increase in electron temperature led to lower SRS gains due to Landau damping of the electron plasma waves. Figure 7(b) shows a typical measured SBS spectrum. The backscattered light wavelength was initially shifted to the red, but the red-shift decreased with time; however, in the gain spectrum predicted with HYDRA and NEWLIP [Fig. 7(c)], the streak shifted steadily towards the red. In the absence of a flow parallel to the interaction beam, the scattered light frequency ω_s is given by frequency and wavenumber
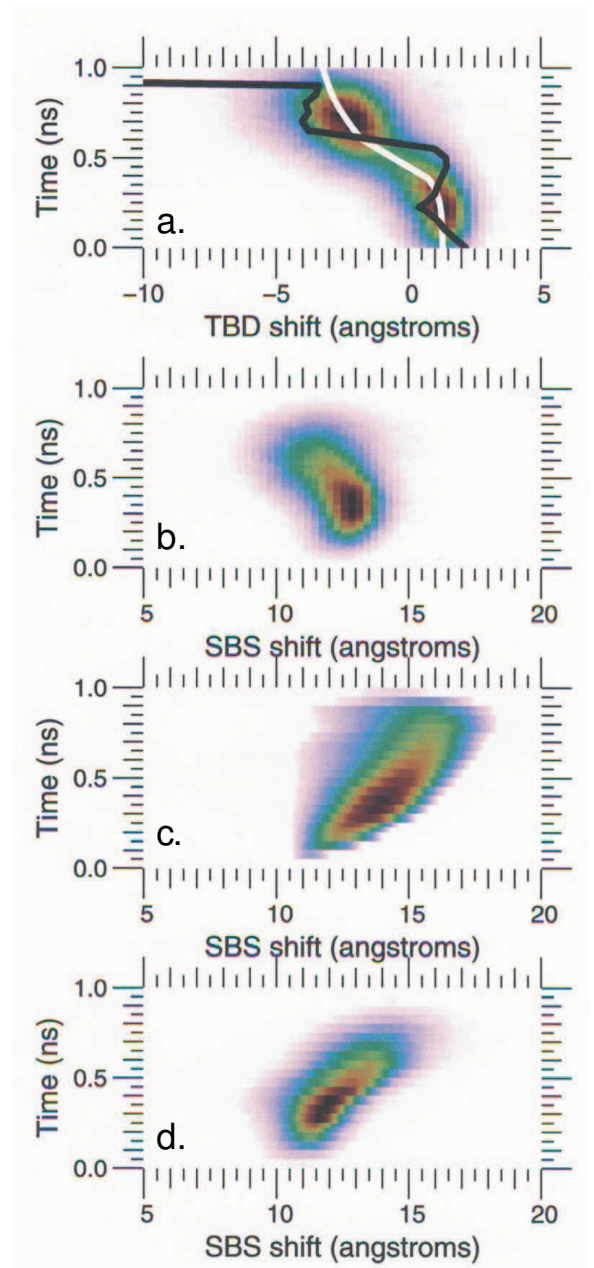

FIG. 7: (Color online). (a) The transmitted light spectrum from an OMEGA hohlraum with a 2ω interaction beam shifted towards the blue in time. (b) The measured SBS spectrum appeared to shift towards the blue in time. (c) The simulated SBS spectrum shifted towards the red as T_e increased. (d) The measured SBS spectrum shifts towards the red in time when corrected for the DAW shift.

matching conditions [22],

$$\omega_s = \omega_0 - \omega_{IAW} \approx \omega_0 - 2k_0 c_s, \qquad (3)$$

where ω_{IAW} is the frequency of the ion acoustic wave, c_s is the sound speed, and ω_0 and k_0 are the frequency and wavenumber of the incident pump. Since $c_s \propto \sqrt{T_e}$,

the scattered light frequency should have dropped as the temperature increased.

The frequency of the transmitted light as measured in the TBD also shifted towards the blue over time [Fig. 7(a)]. The frequency shift was due to the time-dependent change in the phase velocity of the laser light in the plasma [23], given by

$$\Delta\omega = -\frac{\partial}{\partial t}\int_0^L \frac{\omega_0}{c}\sqrt{1-\frac{n_e}{n_c}}dx, \qquad (4)$$

where L is the length of the plasma. We refer to this shift as the "DAW effect," after the authors of [23]. The DAW effect shifts the frequency of the incident pump wave and that of the scattered light wave. For simplicity, we assume that the SBS originated in the middle of the plasma, so the SBS spectrometer measured $\omega_s = \omega_0 - 2k_0 c_s + \Delta\omega$. After removing the measured $\Delta\omega$ from the measured backscattered light frequency, we see that the SBS spectrum does indeed shift to the red, as predicted.

We have incorporated Eq. (4) into NEWLIP. In Fig. 7(a), the wavelength of peak measured transmission at each time (white) and the predicted shift from HY-DRA and NEWLIP (black) both shifted to the blue by 5 Å between 0.5 and 1.0 ns. This level of agreement supports the DAW effect as a plausible explanation for the observed TBD and SBS spectra. Measurements of this effect in future experiments can provide another test of radiation-hydrodynamics code accuracy. Note that the DAW shift is too small to be resolved in SRS spectral measurements.

Recent campaigns used a 3ω interaction beam. These experiments are explained in more detail in a companion paper [24]. These hohlraums had gas fills of $n_e \approx 0.06\, n_c\,(3\omega)$ and were heated with 15 kJ of heater beam energy. The transmission calculated by HYDRA agreed very well with the sum of the SBS backscatter and the transmitted light for the first 1 ns of the laser pulse, another indication that HYDRA accurately calculated the plasma conditions inside the hohlraum (see Ref. [24], Fig. 6). As shown in Fig. 8(a), the TBD measured a frequency shift in the transmitted light. HYDRA and NEWLIP again reproduced this shift. A typical measured SBS backscatter spectrum compared favorably to the gain spectrum from HYDRA and NEWLIP [Fig. 8(b)–(c)], confirming that the SBS is coming from the plateau. The DAW shift was a small correction to the SBS spectrum.

IV. LINEAR GAIN AS A RISK METRIC

We empirically assess the utility of linear gain by plotting measured reflectivity versus calculated backscatter gain. We examine the gas-filled hohlraum described above, as it reached an electron temperature regime relevant to NIF ignition hohlraums. The uncertainty associated with measuring the reflectivity and calculating the gain is quite low for these targets [7]. Figure 9 shows
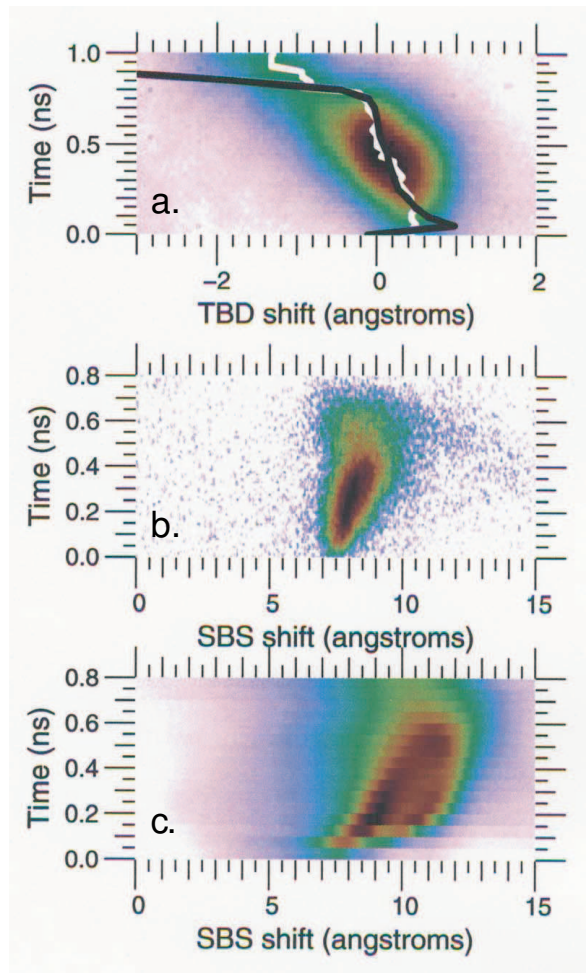

FIG. 8: (Color online). (a) The transmitted light spectrum from an OMEGA hohlraum with a 3ω interaction beam shifted towards the blue in time. The white line shows the wavelength of peak transmission at each time. The simulated shift from HYDRA and NEWLIP (black) agreed well with the experimental shift. (b) The measured SBS spectrum (log scale) is similar to the simulated spectrum (c), which has been corrected for the DAW shift.

the peak gain $G(\omega_s)$ versus time as calculated by HYDRA and NEWLIP for shots with $I \approx 1.9 \times 10^{15}$ W/cm^2, along with the average (simulated) electron temperature along the hohlraum channel. The gain calculations used a 1 ns-long trapezoidal pulse with a rise-time of 0.17 ns for the interaction beam, similar to measured pulses. Figure 9 also shows G versus time for shots with $I \approx 1.3 \times 10^{15}$ W/cm^2.

The gain versus time predicts that the SBS will occur early in the pulse and will shut off as T_e rises. Since the gain peaked early, the onset of SBS in this hohlraum target was very sensitive to the timing of the interaction beam relative to the heater beams. In Fig. 9, increasing the laser-beam start time t_0 from 0.1 ns to 0.4 ns drops the peak gain from $G = 73$ to $G = 32$. To reduce the un-
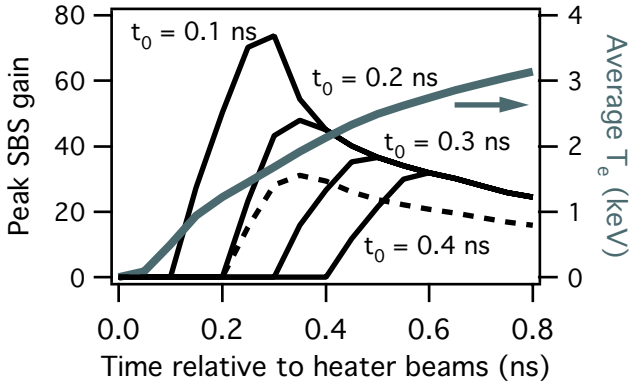
FIG. 9: The peak gain $G(t)$ in an OMEGA hohlraum with a 3ω interaction beam of intensity $I \approx 1.9 \times 10^{15}$ W/cm^2 is high early in time when the electron temperature (gray) is low. The predicted SBS growth is very sensitive to the start time t_0 of the laser pulse. The gain for intensity $I \approx 1.3 \times 10^{15}$ W/cm^2 is also shown (black dashed)
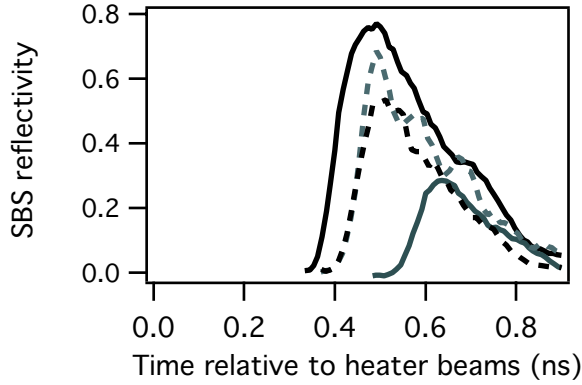

FIG. 11: A reconstructed plot of SBS reflectivity versus gain G shows qualitatively linear growth. The open circles ∘ and black squares ■ correspond to the $I \approx 1.9 \times 10^{15}$ W/cm^2 shots in Fig. 10 with $t_0 = 0.2$ ns and $t_0 = 0.4$ ns, respectively. The open squares and gray circles correspond to the $I \approx 1.3 \times 10^{15}$ W/cm^2, $t_0 = 0.2$ ns shots in Fig. 10. The Tang curve (solid black) is shown for comparison.

FIG. 10: The SBS reflectivity in an OMEGA hohlraum with a 3ω interaction beam of intensity $I \approx 1.9 \times 10^{15}$ W/cm^2 and $t_0 = 0.2$ ns (solid black) peaked early in time. A second shot with $t_0 = 0.4$ ns gave much less total SBS. Two shots with intensity $I \approx 1.3 \times 10^{15}$ W/cm^2 and $t_0 = 0.2$ ns (dashed black and dashed gray) are also shown.

certainty introduced by the sensitivity to t_0, a hohlraum shot was repeated with a delayed interaction beam. Figure 10 compares the measured SBS versus time for a shot with $t_0 = 0.2$ ns to one with $t_0 = 0.4$ ns. These shots did not use PS or SSD and had peak vacuum intensities of $I \approx 1.9 \times 10^{15}$ W/cm^2. The SBS in both shots died away at $t > 0.8$ ns, when $T_e > 3$ keV. This pair of shots suggests that after a brief (100 ps) transient, the backscatter responded to the instantaneous intensity of the interaction beam. Figure 10 also shows the SBS versus time for two shots with $t_0 = 0.2$ ns and $I \approx 1.3 \times 10^{15}$ W/cm^2. One of these shots had no SSD, while the other had 3 Å of SSD. SSD appears to have little effect on reflectivity in this target.

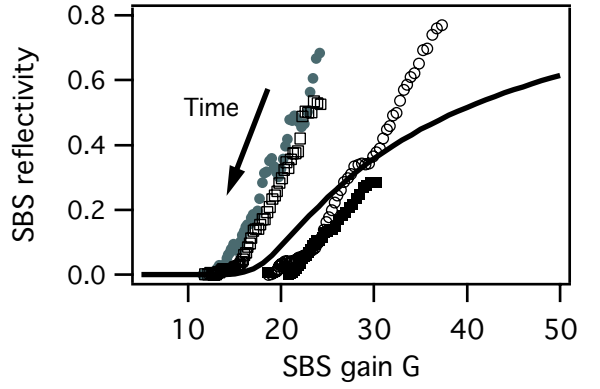We have constructed a plot of reflectivity versus gain

by plotting the measured SBS versus time from Fig. 10 against the calculated gain versus time from Fig. 9. This reconstruction is show in Fig. 11. For comparison purposes, we show the reflectivity R from the "Tang curve" (linear growth and pump depletion only [25]), given by the implicit equation

$$R(1 - R) = \epsilon \, e^{G(1-R)}. \tag{5}$$

In Eq. (5), we take the seed intensity $\epsilon = 10^{-9}$, corresponding to the Thomson scattering reflectivity.

The arrow on Fig. 11 indicates the direction of time. For all the shots, the SBS reflectivity appears to take 50-100 ps to grow, i.e., there is little reflectivity at early time in Fig. 10, even though the gain is quite high in Fig. 9. It is possible that this is due to timing jitter between the interaction beam pulse and the SBS diagnostic. As the temperature rises, the gain drops and the SBS dies away. Note that the low-gain "threshold" regions of Fig. 11 originate late in time, when $G(t)$ is smooth and the experimental and calculational uncertainties are low. The high-gain "saturation" regions of Fig. 11 originate early in time, when uncertainties are very high.

The behavior seen in these experiments is qualitatively consistent with linear growth, although the filamentation instability appears to play a role in the SBS reflectivity. The two shots with $I \approx 1.3 \times 10^{15}$ W/cm^2 show a threshold gain of $G = 12$, whereas the two shots with $I \approx 1.9 \times 10^{15}$ W/cm^2 show a threshold at $G = 20$. As the intensity of the beam was increased, it began to spray beyond the original f-cone (see Ref. [26], Fig. 5). Beam spray may reduce the global (envelope) intensity, effectively reducing the SBS gain G. This will be the subject of future investigation.

The key result of Fig. 11 is that experiments in a long plasma ($\gtrsim$ 10 speckles) at ignition hohlraum relevant

electron temperature exhibited qualitatively linear SBS growth for low reflectivity ($R < 40$ %). One strategy for achieving low backscatter in ignition hohlraums is to keep the laser intensity inside the hohlraum as low as possible. If the amplitudes of the driven plasma waves are sufficiently low, the backscatter will occur in the linear regime, where further beam smoothing and intensity reduction can be most effective. The trend seen in Fig. 11 supports this strategy for designing ignition hohlraums with low backscatter risk.

V. CONCLUSIONS

We have presented detailed comparisons of radiation-hydrodynamics simulations to experimental data from a wide variety of laser-heated targets. The radiation-hydrodynamics code HYDRA agreed well with x-ray emission images of gasbag targets and Thomson scattering data from gasbag and hohlraum targets. The combination of HYDRA and the linear gain postprocessor NEWLIP was able to reproduce spectral features observed in backscattered light and transmitted light data. The

agreement between simulation and experiment indicates that HYDRA simulations can predict the bulk plasma conditions inside laser-heated targets and validates the use of backscattered light spectra as a diagnostic of plasma conditions. We have also found that the SBS measured from OMEGA hohlraums with ignition hohlraum relevant electron temperatures is consistent with linear growth for reflectivity $R < 40$ %. These results validate the use of linear gain postprocessing of ignition hohlraum simulations for assessing backscatter risk in ignition hohlraums.

[1] G. H. Miller, E. I. Moses, and C. R. Wuest, Opt. Eng. **43**, 2841 (2004).

[2] J. D. Lindl, P. Amendt, R. L. Berger, S. G. Glendinning, S. H. Glenzer, S. W. Haan, R. L. Kauffman, O. L. Landen, and L. J. Suter, Phys. Plasmas **11**, 339 (2004).

[3] See ibid, pp. 366-381 for a discussion of LPI modeling capabilities.

[4] M. M. Marinak, G. D. Kerbel, N. A. Gentile, O. Jones, D. Munro, S. Pollaine, T. R. Dittrich, and S. W. Haan, Phys. Plasmas **8**, 2275 (2001).

[5] See National Technical Information Service Document No. UCRL52276 (W. A. Lokke and W. H. Grasberger, XSNQ-U: A non-LTE emission and absorption coefficient subroutine, 1977). Copies may be ordered from the National Technical Information Service, Springfield, VA 22161.

[6] G. P. Schurtz, P. D. Nicolaï, and M. Busquet, Phys. Plasmas **7**, 4238 (2000).

[7] D. H. Froula, J. S. Ross, L. Divol, N. Meezan, A. J. MacKinnon, R. Wallace, and S. H. Glenzer, Phys. Plasmas **13**, 052704 (2006).

[8] Nearly all of the simulations performed for the NOVA technical contract used flux-limited thermal electron conduction with $f = 0.05$. See J. D. Lindl, P. Amendt, R. L. Berger, S. G. Glendinning, S. H. Glenzer, S. W. Haan, R. L. Kauffman, O. L. Landen, and L. J. Suter, Phys. Plasmas **11**, 339 (2004).

[9] G. Gregori, S. H. Glenzer, J. Knight, C. Niemann, D. Price, D. H. Froula, M. J. Edwards, R. P. J. Town, A. Brantov, W. Rozmus, et al., Physical Review Letters **92**, 205006 (2004).

[10] N. B. Meezan, L. Divol, M. M. Marinak, G. D. Kerbel, L. J. Suter, R. M. Stevenson, G. E. Slark, and K. Oades, Phys. Plasmas **11**, 5573 (2004).

[11] See National Technical Information Service Document No. DE200110420 (E. A. Williams, "Platform-Independent Laser-Plasma Interaction Postprocessor for LASNEX", in Lawrence Livermore National Laboratory ICF Annual Report UCRL-L R-105820-98, 13, 1998). Copies may be ordered from the National Technical Information Service, Springfield, VA 22161.

[12] J. F. Drake, P. K. Kaw, Y. C. Lee, G. Schmid, C. S. Liu, and M. N. Rosenbluth, Phys. Fluids **17**, 778 (1974).

[13] D. W. Forslund, J. M. Kindel, and E. L. Lindman, Phys. Fluids **18**, 1002 (1975).

[14] M. J. Norman, J. E. Andrew, T. H. Bett, R. K. Clifford, J. E. England, N. W. Hopps, K. W. Parker, K. Porter, and M. Stevenson, Appl. Opt. **41**, 3497 (2002).

[15] R. M. Stevenson, L. J. Suter, K. Oades, W. Kruer, G. E. Slark, K. B. Fournier, N. Meezan, R. Kauffman, M. Miller, S. Glenzer, et al., Phys. Plasmas **11**, 2709 (2004).

[16] T. H. Bett, C. N. Danson, P. Jinks, D. A. Pepler, I. N. Ross, and R. M. Stevenson, Appl. Opt. **34**, 4025 (1995).

[17] T. R. Boehly, R. S. Craxton, T. H. Hinterman, J. H. Kelly, T. J. Kessler, S. A. Kumpan, S. A. Letzring, R. L. McCrory, S. F. B. Morse, W. Seka, et al., Rev. Sci. Instrum. **66**, 508 (1995).

[18] C. Niemann, L. Divol, D. H. Froula, G. Gregori, O. Jones, R. K. Kirkwood, A. J. MacKinnon, N. B. Meezan, J. D. Moody, C. Sorce, et al., Phys. Rev. Lett. **94**, 085005 (2005).

[19] G. Gregori, S. Glenzer, H.-K. Chung, D. Froula, R. Lee, N. Meezan, J. Moody, C. Niemann, O. Landen, and B. Holst, J. Quant. Spectrosc. Radiat. Transfer **99**, 225 (2006).

[20] One (physical) property of many nonlocal models is that the heat flux reduction relative to classical increases as

the gradient length-scale gets smaller than the thermal mean-free-path. See Fig. 3 in G. P. Schurtz, P. D. Nicolaï, and M. Busquet, Phys. Plasmas **7**, 4238 (2000). When using a stastical laser raytrace model, this can be problematic: If a zone is super-heated due to ray statistics, transport from that zone will practically shut off, resulting in random spatial variations in the electron temperature.

[21] R. L. Berger, C. Constantin, L. Divol, N. Meezan, D. H. Froula, S. H. Glenzer, L. J. Suter, and C. Niemann, Physics of Plasmas **13**, 092702 (2006).

[22] W. L. Kruer, *The Physics of Laser Plasma Interactions*, 87 (Westview Press, 2003).

[23] T. Dewandre, J. R. Albritton, and E. A. Williams, Phys. Fluids **24**, 528 (1981).

[24] D. H. Froula, L. Divol, N. B. Meezan, S. Dixit, P. Neumayer, J. D. Moody, B. B. Pollock, J. S. Ross, L. Suter, and S. H. Glenzer, "Laser beam propagation through inertial confinement fusion hohlraum plasmas," submitted to Phys. Plasmas.

[25] C. L. Tang, J. Appl. Phys. **37**, 2945 (1966).

[26] D. H. Froula, L. Divol, N. B. Meezan, S. Dixit, J. D. Moody, B. B. Pollock, J. S. Ross, and S. H. Glenzer, "Ideal laser beam propagation through high temperature ignition hohlraum plasmas," to be published in Phys. Rev. Lett.